*Journal of Modern Optics*
Vol. 55, No. 9, 20 May 2008, 1441–1462

Taylor & Francis
Taylor & Francis Group

# On an approach for improving the range resolution of pulsed coherent Doppler lidars

Ljuan L. Gurdev* and Tanja N. Dreischuh

*Institute of Electronics, Bulgarian Academy of Sciences, Sofia, Bulgaria*

(*Received 15 May 2007; final version received 5 September 2007*)

As a result of an analysis of the autocovariance of the complex heterodyne lidar signal, some general-enough inverse techniques (algorithms) are derived for recovering with high range resolution, below the sensing pulse length, of Doppler-velocity profiles in the atmosphere. Unlike our preceding works, it is assumed here that the laser pulses can have arbitrary fluctuating shape. The presence is also supposed of possible regular, arbitrary in form, intrapulse frequency deviations (chirp) and random frequency, phase and radial (Doppler)-velocity fluctuations. The algorithm performance and efficiency are studied and illustrated by computer simulations, taking into account the influence of the chirp and various random factors such as additive noise, pulse-shape fluctuations and radial-velocity fluctuations. It is shown that the algorithms developed allow the Doppler-velocity profiles to be determined with a considerably shorter resolution interval compared with the pulse length, at a reasonable number of signal realizations (laser shots) and appropriate data processing to reduce the statistical error due to the random factors.

**Keywords:** lidar remote sensing; coherent doppler lidar; range resolution; Doppler-velocity profiles

## 1. Introduction

Pulsed coherent Doppler lidars are intensively developed nowadays as sensitive instruments for measuring with high range resolution the profiles of the radial (Doppler) velocity of atmospheric wind. It is usually accepted that the minimum achievable range resolution interval $R$ is of the order of the sensing laser pulse length $l_p$ (e.g. [1,2]). Based on this conception, a way to improve the range resolution is to use shorter laser pulses. However, the pulse length is reciprocally related with an uncertainty $\Delta v$ in the determination of the Doppler velocity $v$ so that $R\Delta v \sim c\lambda$, where $c$ is the speed of light and $\lambda$ is the wavelength of the sensing radiation [3]. In this case, to improve the range resolution without lowering the velocity measurement sensitivity one should use shorter pulses of proportionally shorter-wavelength radiation. For instance, one can reach a five-times

*Corresponding author. Email: lugurdev@ie.bas.bg

ISSN 0950–0340 print/ISSN 1362–3044 online

DOI: 10.1080/09500340701668564
http://www.informaworld.com

better resolution by using laser pulses with $\lambda = 2\,\mu m$ instead of five times longer pulses with $\lambda = 10.6\,\mu m$.

By using a different approach, we recently developed some novel techniques for retrieving Doppler-velocity profiles with a resolution scale that is much less than the pulse length [4,5]. The approach is based on an analysis of the coherent heterodyne signal autocovariance, assuming that the pulse shape, the pulse-shape fluctuation statistics, and the regular intrapulse frequency chirp are known (experimentally determined). The retrieval techniques (algorithms) developed so far concern the cases of rectangular and rectangular-like [4] as well as exponentially-shaped [5,6] laser pulses with arbitrary frequency chirp and stationary relative pulse-shape fluctuations. The main purpose of the present study is to develop, and examine by simulations, some general enough such techniques for pulses with arbitrary chirp and arbitrary smooth shape with nonstationary relative fluctuations. The analysis conducted is based on a general expression of the heterodyne-signal autocovariance that is described and discussed in Section 3. A brief analytical description of the signal itself is given in Section 2. The retrieval algorithms are derived and discussed in Section 4. In Section 5 we have presented and discussed the results from the computer simulations that illustrate the potentialities and the limitations of the algorithms derived in the paper. The main results obtained in the study are summarized in Section 6.

## 2. Coherent heterodyne lidar signal

As in our preceding works [4–6] we consider the sensing radiation as a sequence of quasi-monochromatic laser pulses with basic frequency $\omega_0$, dimensionless temporal amplitude envelope $f_0(\vartheta)$, regular (chirp) and random frequency deviations $\delta\omega_{ch}(\vartheta)$ and $\delta\omega_r(\vartheta)$, respectively, and random phase fluctuations $\varphi_r(\vartheta)$ around some mean phase constant $\varphi_0$; $\vartheta$ is a time variable. The fluctuations $\delta\omega_r(\vartheta)$ and $\varphi_r(\vartheta)$ are assumed to be mutually uncorrelated stationary random processes with, respectively, mean values $\langle\delta\omega_r\rangle = 0$ and $\langle\varphi_r\rangle = 0$, symmetric probability density distributions $p(\delta\omega_r) = p(-\delta\omega_r)$ and $p(\varphi_r) = p(-\varphi_r)$, and autocorrelation times $\tau_\omega$ and $\tau_\varphi$; $\langle\cdot\rangle$ denotes ensemble average. The chirp $\delta\omega_{ch}(\vartheta)$ is considered as arbitrary in form but as a differentiable function of $\vartheta$. The sensing laser pulses are supposed to have arbitrary smooth shape with asymptotically falling tail such that $f_0(\vartheta) \equiv 0$ for $\vartheta \le 0$, and $f_0(\vartheta) \to 0$ for $\vartheta \to \infty$. The pulse power shape $P_{imp}(\vartheta)$ can be written in the form

$$P_{imp}(\vartheta) = P_p f(\vartheta), \tag{1}$$

where $P_p$ is the pulse peak power, and $f(\vartheta) = f_0^2(\vartheta)$; the peak values of functions $f(\vartheta)$ and $f_0(\vartheta)$ are equal to unity. To describe the pulse shape fluctuations one may represent function $f_0(\vartheta)$ as

$$f_0(\vartheta) = f_{0m}(\vartheta)[1 + \kappa(\vartheta)], \tag{2}$$

where $f_{0m}(\vartheta) = \langle f_0(\vartheta)\rangle$ is the ensemble-mean pulse envelope, and $\kappa(\vartheta) = [f_0(\vartheta) - f_{0m}(\vartheta)]/f_{0m}(\vartheta)$ is a random function representing the envelope relative fluctuations. Then the autocovariance of $f_0(\vartheta)$ is

$$\langle f_0(\vartheta) f_0(\vartheta+\theta)\rangle = f_{0m}(\vartheta) f_{0m}(\vartheta+\theta)[1 + g(\vartheta,\theta)], \tag{3a}$$

where $g(\vartheta,\theta) = \langle \kappa(\vartheta)\kappa(\vartheta+\theta)\rangle$ is the fluctuation autocovariance that depends in general not only on the time shift $\theta$ but on the variable $\vartheta$ as well. Then the fluctuation variance $\eta(\vartheta) = g(\vartheta,\theta=0) = \langle \kappa^2(\vartheta)\rangle$ also depends on $\vartheta$. In the particular case of stationary fluctuations the autocovariance is independent of $\vartheta$, and the variance is constant, i.e. $g(\vartheta,\theta) \equiv g(\theta)$, and $\eta = g(\theta=0) = \text{const}$. The mean-square envelope $f_m(\vartheta) = \langle f(\vartheta)\rangle = \langle f_0^2(\vartheta)\rangle$ is obtainable from Equation (3a) in the form

$$f_m(\vartheta) = f_{0m}^2(\vartheta)[1 + \eta(\vartheta)]. \tag{3b}$$

On the basis of Equations (2) and (3b) it is not difficult to show that if $\widehat{f_m}(\vartheta)$ is a statistical estimate of $f_m(\vartheta)$, say arithmetic mean over $N$ pulse realizations, its relative standard deviation $\Delta\widehat{f_m}(\vartheta) = \langle[\widehat{f_m}(\vartheta) - f_m(\vartheta)]^2/f_m^2(\vartheta)\rangle^{1/2}$ is equal in practice to $2[\eta(\vartheta)/N]^{1/2}$. We shall further model (in Section 5) the waveform $f_0(\vartheta)$ without requiring it to have unitary peak value. This means in fact that the simulations will involve not only pulse shape fluctuations but pulse peak power fluctuations as well (see Equation (1)).

Let us further assume that the lidar return (the backscattered laser radiation) is a result of incoherent single scattering from atmospheric aerosol particles. In this case the coherent heterodyne lidar signal (the complex signal photocurrent) $I(t)$, for each given realization of the atmospheric conditions and the sensing laser pulse, can be considered [7] as a zero-mean circular complex conditionally-Gaussian random quantity $I(t) = J(t) + \mathrm{j}Q(t)$, where $J(t)$ and $Q(t)$ are, respectively, in-phase and quadrature signal components, $t$ is the moment of detection (after the pulse emission), and j is the imaginary unit. The signal profile $I(t = 2z/c)$, along the lidar line of sight (LOS) $0z$, is then expressible in the form [5]:

$$I(t=2z/c) = \exp\{\mathrm{j}[\varphi_0 - \varphi_h(t)]\} \sum_{l=l_1+1}^{l_2} f_0(t - 2z_l/c)\,\mathrm{d}\mathcal{A}(z_l) \times \exp\left\{\mathrm{j}\omega_{im}(z_l)t + \mathrm{j}\varphi_{\omega d}[(t-2z_l/c)\chi_0(z_l)] + \mathrm{j}\varphi_r[(t-2z_l/c)\chi_0(z_l)]\right\}, \tag{4}$$

where $z = ct/2$ is the LOS pulse-front position corresponding to the moment of detection $t$; $l$ is the number of the elementary aerosol slice between two adjacent transversal planes $z = (l-1)\Delta z$ and $z = l\Delta z$, $\Delta z$ is an elementary step along the LOS, $z_l = l\Delta z$, $l_1 = z_0/\Delta z$, $l_2 = ct/(2\Delta z)$, $z_0$ is the upper limit of the lidar dead (blind) zone (the lidar return from this zone is not detectable); $\varphi_h(t)$ is the local-oscillator phase fluctuation function supposed to be invariable during a pulse duration; $\omega_{im}(z_l) = \omega_0\chi_0(z_l) - \omega_h$ is the intermediate frequency concerning a current ($l$th) elementary aerosol slice, $\omega_h$ is the local-oscillator frequency, $\chi_0(z_l) = 1 - 2v(z_l)/c$, $v(z_l)$ is the corresponding radial velocity of the aerosol scatterers; $\varphi_{\omega d}[\vartheta] = \varphi_{ch}[\vartheta] + \varphi_{\omega r}[\vartheta]$ is the phase increment due to the chirp and the random frequency fluctuations, $\varphi_{ch}[\vartheta] = \int_0^\vartheta \delta\omega_{ch}(\vartheta')\mathrm{d}\vartheta'$ and $\varphi_{\omega r}[\vartheta] = \int_0^\vartheta \delta\omega_r(\vartheta')\mathrm{d}\vartheta'$; $\mathrm{d}\mathcal{A}(z_l) = [\Phi_c(z_l)\Delta z]^{1/2} w_l$ is a random differential quantity, where $w_l = w = w_r + \mathrm{j}w_i$ is a circular complex Gaussian random quantity with zero mean value $\langle w\rangle = 0$

($\langle w_r\rangle = \langle w_i\rangle = 0$) and unitary variance $Dw = \langle ww^*\rangle = 1$ ($\langle w_r^2\rangle = \langle w_i^2\rangle = 1/2$), and $\Phi_c(z_l)$ describes (see below) the contribution of unitary 'scattering length' along the LOS to the conditional mean signal power at each given realization of the laser pulse and the atmospheric conditions.

## 3. Autocovariance of the coherent heterodyne lidar signal

With respect to the time variable $t$ (or the range variable $z = ct/2$) the signal $I(t)$ is in general a non-stationary (inhomogeneous) random function whose autocovariance $\mathrm{Cov}(t,\theta) = \langle I^*(t)I(t+\theta)\rangle$ depends not only on the time shift $\theta$ but on the moment $t$ as well. For a positive time shift $\theta \geq 0$ the autocovariance function $\mathrm{Cov}(t,\theta)$ is obtainable from Equation (4) in the following continuous form [5,6]:

$$\mathrm{Cov}(t,\theta) = \int_{z_0}^{ct/2} \mathrm{d}z' \,\langle f_0(t-2z'/c) f_0(t+\theta-2z'/c)\rangle\, \Phi(z') \times \exp\{\mathrm{j}[\omega_m(z')\theta] + \delta\omega_{ch}(t-2z'/c)\theta\}\zeta(\theta)\xi(\theta)\gamma(z', 2\omega_0\theta/c), \tag{5}$$

where $\omega_m(z') = \langle\omega_{im}(z')\rangle = \omega_0\chi(z') - \omega_h$, $\chi(z') = 1 - v_m(z')/c$, and $v_m(z') = \langle v(z')\rangle$ is the ensemble-mean radial-velocity profile along the LOS; $\Phi(z') = \langle\Phi_c(z')\rangle$; $\zeta(\theta) = \langle\exp(\mathrm{j}\delta\omega_r\theta)\rangle$ and $\xi(\theta) = \langle\exp(\mathrm{j}\varphi_r^{\mathrm{I}}\theta)\rangle$ are real characteristic functions of the frequency fluctuations $\delta\omega_r(\vartheta)$ and the differentiated realizations $\varphi_r^{\mathrm{I}}(\vartheta)$ of the phase fluctuations $\varphi_r(\vartheta)$ in the sensing laser pulse; $\gamma(z', q = 2\omega_0\theta/c) = \langle\exp[\mathrm{j}q\tilde{v}(z')]\rangle$ is a real characteristic function of the symmetrically-distributed turbulent velocity fluctuations $\tilde{v}(z') = v(z') - v_m(z')$ (here the superscript 'I' denotes differentiation with respect to $\vartheta$). When deriving Equation (5) it is assumed that all the random factors of importance are statistically stationary and the averaging involves the full set (parent population) of signal realizations. At $\theta = 0$ Equation (5) leads to the following expression of the ensemble-mean signal power profile $P(t = 2z/c) = \mathrm{Cov}(t = 2z/c, 0) = \langle|I(t = 2z/c)|^2\rangle$:

$$P(t = 2z/c) = \int_{z_o}^{ct/2} f_m(t - 2z'/c)\Phi(z')\mathrm{d}z'. \tag{6}$$

At known (experimentally determined) forms of $P(t)$ and $f(\vartheta)$, on the basis of Equation (6) one can recover the profile of $\Phi(z')$ by using deconvolution techniques [8]. Equation (6) reveals as well the sense of function $\Phi(z')$ as characterizing the contribution of unitary length along the LOS to $P(t = 2z/c)$ that is an average supposed over all the realizations of the atmospheric conditions and the sensing laser pulse. Correspondingly, the profile of $\Phi(z') = \langle\Phi_c(z')\rangle$ is an average over the realizations of all the determinant random factors such as the atmospheric extinction and (aerosol) backscattering, the atmospheric refractive turbulence, and the laser pulse peak power. The explicit expression of $\Phi(z)$ is $\Phi(z) = \alpha\langle P_p\rangle\eta(z)z^{-2}\beta(z)\mathcal{T}^2(z)$, where $\alpha$ is a lidar constant, and $\eta(z)$, $\beta(z)$ and $\mathcal{T}(z)$ are, respectively, the receiving (heterodyne) efficiency, and the atmospheric backscattering coefficient and transmittance (e.g. [2,8,9]). When the pulse length is much less than the least variation scale of $\Phi(z')$, instead of Equation (6) we obtain that $P(t = 2z/c) \cong P_{sh}(t = 2z/c) = (c\tau_p/2)\Phi(z = ct/2)$, where $\tau_p = \int_0^\infty f(\vartheta)\mathrm{d}\vartheta$ is an effective pulse duration, and $l_p = c\tau_p$ is the corresponding effective pulse length. The profile of $P_{sh}(t = 2z/c)$ which

is obviously proportional to $\Phi(z)$ may be called the maximum-resolved or the short-pulse ($\delta$-pulse) signal power profile because it is obtainable at short-enough ($\delta$-like) laser pulses.

In the case of multishot lidar operation a common autocovariance estimate $\widehat{\mathrm{Cov}}(t,\theta)$ is

$$\widehat{\mathrm{Cov}}(t,\theta) = N^{-1}\sum_{k=1}^{N}[I_k^*(t)+n_k^*(t)][I_k(t+\theta)+n_k(t+\theta)], \tag{7}$$

where $I_k(\vartheta)$ $(k=1,2,\ldots,N)$ are $N$ signal realizations obtained by $N$ laser shots; $n_k(\vartheta)=n_{k,\mathrm{r}}(\vartheta)+\mathrm{j}n_{k,\mathrm{i}}(\vartheta)$ is a complex random quantity whose real and imaginary parts, $n_{\mathrm{r}}(\vartheta)$ and $n_{\mathrm{i}}(\vartheta)$, represent the additive measurement noise in the in-phase and the quadrature lidar channels, respectively. The pulse repetition rate $r$ is supposed to be high enough to ensure, for an observation time $T$, a sufficiently large value of $N=rT$ allowing one to effectively average the random factors disturbing $I_k(t)$ and, respectively, $\widehat{\mathrm{Cov}}(t,\theta)$. The main such factors are: the incoherent-backscattering-due (reflective-speckle) fluctuations, with temporal correlation scales of the order of microseconds [10]; the amplitude, frequency, and phase fluctuations in the sensing laser pulses; the additive measurement noise; the refractive-turbulence-due amplitude and phase signal fluctuations with correlation scales of the order of milliseconds [10,11]; the fluctuations of the scattering particulate matter density, with correlation scales, e.g. of 10 to 400 ms and contrast (the ratio of the standard deviation to the mean value) of 0.03 to 0.15 [12]; as well as the turbulent velocity fluctuations whose correlation time $t_{\mathrm{c}}$ is the largest one and depends on the lifetime, the scales and the mean translational velocity of the turbulent whirls [13, 14]. In the case of an overfilled observation period $T$ we shall suppose here (when $N > T/t_{\mathrm{c}}$), the averaging efficiency is determined by the relation between $T$ and $t_{\mathrm{c}}$ [14,15]. Then the above-mentioned random factors will be entirely averaged only for a too long observation time $T(\gg t_{\mathrm{c}})$, typically of the order of many minutes. Under stationary atmospheric conditions the full-averaging procedure leads to an estimate of the parent-population mean signal autocovariance $\mathrm{Cov}(t,\theta)$ given analytically by Equation (5).

The contemporary powerful-enough pulsed laser transmitters for coherent lidars can have a pulse repetition rate of the order of one kilocycle [16]. Consequently, for a few seconds they can provide a sufficiently large number of signal realizations to essentially average (suppress) the small-scale signal fluctuations of the type of the first five above-listed ones. At the same time the turbulent velocity fluctuations $\tilde{v}$ might not be effectively averaged because of their large mean temporal correlation scale $t_{\mathrm{c}}$. Then the question arises about the validity and the interpretation of Equation (5) for $T \ll t_{\mathrm{c}}$ and $T \sim t_{\mathrm{c}}$. In this case, instead of Equation (5), on the basis of Equations (4) and (7) we obtain that

$$\begin{aligned}\mathrm{Cov}(t,\theta) = {} & \int_{z_0}^{ct/2} \mathrm{d}z' \,\langle f_0(t-2z'/c) f_0(t+\theta-2z'/c)\rangle\, \Phi(z') \\ & \times \exp[\mathrm{j}\delta\omega_{\mathrm{ch}}(t-2z'/c)\theta]\zeta(\theta)\xi(\theta)\, Y(z',\theta,T) + o(N^{-1/2}),\end{aligned} \tag{8}$$

where $Y(z',\theta,T) = N^{-1}\sum_{k=1}^{N}\exp[\mathrm{j}\omega_{\mathrm{m},k}(z')\theta]$, $\omega_{\mathrm{m},k}(z') = \omega_0[1-2v_k(z')/c]-\omega_{\mathrm{h}}$, $v_k(z') = v[z',(k-1)\Delta\tau]$ is the realization of the radial-velocity profile at the $k$th laser shot, and $\Delta\tau = T/N = r^{-1}$ is the time interval between two adjacent laser shots. Here all the random factors of importance, with the exception of $v(z)$, are supposed to fluctuate stationary from

pulse to pulse within the period $T$. It was deduced formerly, on the basis of qualitative physical considerations [6] and analytically [14], that the signal autocovariance $\mathrm{Cov}(t,\theta)$, given by Equation (5) or Equation (8), contains information about and allows one to determine a mean, for the period $T$, range-resolved Doppler-velocity profile $v_\mathrm{r}(z)$. For a long-term measurement procedure (under stationary conditions), when $T \gg t_\mathrm{c}$, this profile is an estimate of the ensemble-mean Doppler-velocity profile $v_\mathrm{m}(z)$. For a short-term measurement procedure, when $T \ll t_\mathrm{c}$, it should coincide with a near instantaneous Doppler-velocity profile, i.e. $v_\mathrm{r}(z) \cong v_1(z) \cong v_k(z)$.

## 4. Retrieving high-resolution Doppler-velocity profiles

The problem to be solved here is to determine and interpret the character of the profile $v_\mathrm{r}(z = ct/2)$ at known (experimentally determined) $\widehat{\mathrm{Cov}}\,(t,\theta)$, $\delta\omega_\mathrm{ch}(\vartheta)$, and $f_\mathrm{m}(\vartheta) = \langle f_0^2(\vartheta)\rangle$. The possibility of solving this problem is explained physically [5] by the fact that when moving along the LOS, the sensing laser pulse involves successively new elementary aerosol slices of the scattering medium. Therefore, two adjacent values of the signal, $I(t)$ and $I(t+\Delta t)$ ($\Delta t = 2\Delta z/c \ll \tau_\mathrm{p}$), differ in the information involved about the properties of the slice between $z = ct/2$ and $z = c(t+\Delta t)/2$. This information may be extracted in principle by some differentiating procedure, but as the signal has a stochastic nature one should differentiate some statistical moments of it. To obtain the Doppler-velocity profiles, one should use statistical moments containing phase information. Such a moment is the signal autocovariance $\mathrm{Cov}(t,\theta)$ described mathematically by Equation (5) or Equation (8).

On the basis of Equation (5) we obtain the following expression of the imaginary part $\mathcal{R}(t) = \mathrm{Im}\,\mathrm{Cov}_\theta^\mathrm{I}(t,\theta=0)$ of the first derivative $\mathrm{Cov}_\theta^\mathrm{I}(t,\theta=0)$ of $\mathrm{Cov}(t,\theta)$ with respect to $\theta$ at $\theta = 0$:

$$\mathcal{R}(t) = \int_{z_0}^{ct/2} \mathrm{d}z' \Phi(z') \mathcal{F}(t - 2z'/c) + \int_{z_0}^{ct/2} \mathrm{d}z' \mathcal{H}(z') f_\mathrm{m}(t - 2z'/c), \tag{9}$$

where $\mathcal{F}(t-2z'/c) = f_\mathrm{m}(t-2z'/c)\delta\omega_\mathrm{ch}(t-2z'/c)$, and $\mathcal{H}(z') = \omega_\mathrm{m}(z')\Phi(z')$. When deriving Equation (9), it is taken into account that $\zeta(\theta=0) = \xi(\theta=0) = \gamma(z',\theta=0) = 1$, and (the first derivatives with respect to $\theta$ at $\theta = 0$) $\zeta_\theta^\mathrm{I}(\theta=0) = \mathrm{j}\langle\delta\omega_\mathrm{r}\rangle = 0$, $\xi_\theta^\mathrm{I}(\theta=0) = \mathrm{j}\langle\varphi_\mathrm{r}^\mathrm{I}\rangle = 0$ and $\gamma_\theta^\mathrm{I}(z',\theta=0) = 2(\omega_\mathrm{o}/c)\langle\tilde{v}(z')\rangle = 0$. The finite integration limits in Equation (9) indicate only the points where the integrand becomes identical to zero. In fact, functions $f_\mathrm{m}(\vartheta = t - 2z'/c)$, $\delta\omega_\mathrm{ch}(\vartheta = t - 2z'/c)$, $\Phi(z')$ and $\omega_\mathrm{m}(z')$, and, respectively, $\mathcal{F}(\vartheta = t - 2z'/c)$ and $\mathcal{H}(z')$, are defined and integrable over the interval $(-\infty, \infty)$. Therefore, one may consider the integration as being performed from $-\infty$ to $+\infty$. Then the Fourier transformation of Equation (9) leads to the relations

$$\tilde{\mathcal{R}}(\Omega) = \tilde{\mathcal{F}}(\Omega)\tilde{\Phi}(k) + \tilde{\mathcal{H}}(k)\tilde{f_\mathrm{m}}(\Omega), \tag{10}$$

i.e.

$$\tilde{\mathcal{H}}(k) = [\tilde{\mathcal{R}}(\Omega) - \tilde{\mathcal{F}}(\Omega)\tilde{\Phi}(k)]\tilde{f_\mathrm{m}}^{-1}(\Omega), \tag{11}$$

where

$$\tilde{\mathcal{R}}(\Omega) = \int_{-\infty}^{\infty} \mathcal{R}(t)\exp(\mathrm{j}\Omega t)\mathrm{d}t, \tag{12a}$$

$$\tilde{\mathcal{F}}(\Omega) = \int_{-\infty}^{\infty} \mathcal{F}(\vartheta)\exp(\mathrm{j}\Omega\vartheta)\mathrm{d}\vartheta, \tag{12b}$$

$$\tilde{f_{\mathrm{m}}}(\Omega) = \int_{-\infty}^{\infty} f_{\mathrm{m}}(\vartheta)\exp(\mathrm{j}\Omega\vartheta)\mathrm{d}\vartheta, \tag{12c}$$

$$\tilde{\mathcal{H}}(k) = \int_{-\infty}^{\infty} \mathcal{H}(z)\exp(\mathrm{j}kz)\mathrm{d}z, \tag{12d}$$

and

$$\tilde{\Phi}(k) = \int_{-\infty}^{\infty} \Phi(z)\exp(\mathrm{j}kz)\mathrm{d}z, \tag{12e}$$

are Fourier transforms, assumed to exist, of $\mathcal{R}(t)$, $\mathcal{F}(\vartheta)$, $f_{\mathrm{m}}(\vartheta)$, $\mathcal{H}(z)$, and $\Phi(z)$, respectively; $k = 2\Omega/c$. From Equation (11), by using the inverse Fourier transformation, we obtain the following algorithm for retrieving $\omega_{\mathrm{m}}(z = ct/2)$:

$$\begin{aligned}\omega_{\mathrm{m}}(z = ct/2) &= [2\pi\Phi(z)]^{-1}\int_{-\infty}^{\infty}\mathrm{d}k[\tilde{\mathcal{R}}(ck/2) - \tilde{\mathcal{F}}(ck/2)\tilde{\Phi}(k)] \\ &\quad\times \tilde{f_{\mathrm{m}}}^{-1}(ck/2)\exp(-\mathrm{j}kz) \\ &= [\pi c\Phi(z)]^{-1}\int_{-\infty}^{\infty}\mathrm{d}\Omega[\tilde{\mathcal{R}}(\Omega) - \tilde{\mathcal{F}}(\Omega)\tilde{\Phi}(2\Omega/c)]\tilde{f_{\mathrm{m}}}^{-1}(\Omega)\exp(-\mathrm{j}\Omega t).\end{aligned} \tag{13}$$

Equation (11) can also be written in the form

$$\mathcal{R}(t) - S(t) = W(t) = \int_{z_0}^{ct/2} f_{\mathrm{m}}(t - 2z'/c)\mathcal{H}(z')\mathrm{d}z', \tag{14}$$

where the term $S(t) = \int_{z_0}^{ct/2}\mathcal{F}(t - 2z'/c)\Phi(z')\mathrm{d}z'$ describes the chirp influence. By using the substitution $t' = 2z'/c$, and double differentiation with respect to $t$, from Equation (14) we obtain

$$\mathcal{H}(ct/2) = \mathcal{L}(t) + \int_{t_0}^{t}\mathcal{K}(t - t')\mathcal{H}(ct'/2)\mathrm{d}t', \tag{15}$$

where $\mathcal{L}(t) = (2/c)W^{\mathrm{II}}(t)/f_{\mathrm{m}}^{\mathrm{I}}(0)$, $\mathcal{K}(t - t') = -f_{\mathrm{m}}^{\mathrm{II}}(t - t')/f_{\mathrm{m}}^{\mathrm{I}}(0)$, $f_{\mathrm{m}}^{\mathrm{I}}(0) = f_{\mathrm{m}}^{\mathrm{I}}(t - t')|_{t=t'}$, $t_0 = 2z_0/c$, and superscripts 'I' and 'II' denote, respectively, first and second derivatives with respect to $t$. Equation (15) is the second kind of Volterra integral equation with respect to $\mathcal{H}(z = ct/2)$. It has a unique continuous solution within the interval $[t_0, t]$ ($[z_0, z]$), when $\mathcal{L}(t)$ is a continuous function within the same interval and the kernel

$\mathcal{K}(t-t')$ is a continuous or square-summable function of $t$ and $t'$ over some rectangle $\{t_0 \le t, t' \le \mathcal{T}\}$. The solution of Equation (15) is obtainable in the form [17]

$$\mathcal{H}(z=ct/2) = \mathcal{L}(t) + \int_0^{t-t_0} \mathcal{R}(\varsigma)\mathcal{L}(t-\varsigma)\mathrm{d}\varsigma, \tag{16}$$

where $\mathcal{R}(\varsigma) = \sum_{i=1}^{\infty} \mathcal{K}_i(\varsigma)$ is the resolvent, $\mathcal{K}_i(\varsigma) = \int_0^{\varsigma} \mathcal{K}_{i-1}(\varsigma')\mathcal{K}_1(\varsigma-\varsigma')\mathrm{d}\varsigma'$, and $\mathcal{K}_1(\varsigma) = \mathcal{K}(\varsigma)$. Equation (16) provides in fact another algorithm for retrieving $\omega_{\mathrm{m}}(z)$ [see the definition of $\mathcal{H}(z=ct/2)$]:

$$\omega_{\mathrm{m}}(z=ct/2) = \mathcal{H}(z=ct/2)/\Phi(z=ct/2). \tag{17}$$

Theoretically, the above-obtained two algorithms [Equations (13) and (17)] allow one to achieve a retrieval resolution cell that is equal to the sampling interval $\Delta z$ (or $\Delta t = 2\Delta z/c$). However, the really-achievable resolution cell is larger (but less than the pulse length) because of the necessity of any type of filtering to additionally suppress the disturbing noise effects. Then the minimum resolution interval $R$ will be already of the order of the width $W$ of the window of the filter employed. To retain a satisfactory range resolution, the value of $W$ should be less than the least variation scale $\Lambda_v$ of the mean radial velocity $v_{\mathrm{m}}(z)$.

As mentioned at the end of Section 3, each radial-velocity profile $v_{\mathrm{r}}(z)$, recovered by using the signal-autocovariance-based inverse techniques developed here and in previous works [4,5], should be considered in general as some mean (for the observation period $T$) range-resolved Doppler-velocity profile; when $T \gg t_{\mathrm{c}}$ (under stationary conditions) or $T \ll t_{\mathrm{c}}$ this profile tends, respectively, to the ensemble-mean or to an instantaneous Doppler-velocity profile. To substantiate explicitly such an interpretation, let us consider, as a basis of analysis, Equation (8) instead of Equation (5). If now we repeat the procedure of deriving Equation (9) we shall obtain the same general result, but with $\omega_{\mathrm{m}}(z)$ having the following explicit form:

$$\omega_{\mathrm{m}}(z) = \omega_0[1 - 2v_{\mathrm{a}}(z)/c] - \omega_{\mathrm{h}}, \tag{18}$$

where

$$v_{\mathrm{a}}(z) = N^{-1}\sum_{k=1}^{N} v_k(z). \tag{19}$$

Thus, the formally-restored [by algorithms (13) and (17)] radial-velocity profile $v_{\mathrm{r}}(z)$ is in general the arithmetic-mean profile $v_{\mathrm{a}}(z)$ over $N$ laser shots during the measurement period $T$. In the case of stationary fluctuations of $v(z)$, when $N = T/\Delta\tau \gg 1$ and $\Delta\tau \ge t_{\mathrm{c}}$, according to the law of averages (see e.g. [18]) the profile $v_{\mathrm{a}}(z)$ is a good estimate of $v_{\mathrm{m}}(z)$ with variance $Dv_{\mathrm{a}} = \langle (v_{\mathrm{a}} - v_{\mathrm{m}})^2 \rangle \sim \sigma_v^2/N \ll \sigma_v^2$, where $\sigma_v^2 = \langle \tilde{v}^2 \rangle$; that is, $v_{\mathrm{a}}(z)$ should practically coincide with $v_{\mathrm{m}}(z)$. When $T/t_{\mathrm{c}} \gg 1$ and $t_{\mathrm{c}} \gg \Delta\tau$ the profile $v_{\mathrm{a}}(z)$ [Equation (19)] can be represented for convenience as $v_{\mathrm{a}}(z) = T^{-1}\int_0^T v(z,\vartheta)\mathrm{d}\vartheta$, and $\tilde{v}_{\mathrm{a}}(z) = v_{\mathrm{a}}(z) - v_{\mathrm{m}}(z) = T^{-1}\int_0^T \tilde{v}(z,\vartheta)\mathrm{d}\vartheta$, where $\tilde{v}(z,\vartheta) = v(z,\vartheta) - v_{\mathrm{m}}(z)$. Then the variance of $v_{\mathrm{a}}(z)$, $Dv_{\mathrm{a}}(z) = \langle \tilde{v}_{\mathrm{a}}^2(z) \rangle$, can be estimated by the following series of relations: $Dv_{\mathrm{a}}(z) = T^{-2}\int\int_0^T \mathrm{d}\vartheta'\,\mathrm{d}\vartheta'' \langle \tilde{v}(z,\vartheta')\tilde{v}(z,\vartheta'') \rangle = (2\sigma_v^2/T)\int_0^T (1-\theta/T)K(z,\theta)\mathrm{d}\theta \approx 2\sigma_v^2 t_{\mathrm{c}}/T \ll \sigma_v^2$,

where $K(z,\theta) = \langle \tilde{v}(z,\vartheta+\theta)\tilde{v}(z,\vartheta)\rangle/\sigma_v^2$ is the correlation coefficient of the radial-velocity fluctuations, and $t_c = \int_0^T K(\theta)\mathrm{d}\theta$ is an estimate of $t_c$. (We have used meanwhile the substitution $\vartheta' = \vartheta'$ and $\theta = \vartheta'' - \vartheta'$ as well as the assumption that $K(\theta)$ is a symmetric function of $\theta$.) Thus, function $v_a(z)$ turns out again to be a good estimate of $v_m(z)$, that is, when $T(N) \to \infty$ $v_a(z)$ tends to $v_m(z)$ with a probability tending to unity. When $T \ll t_c$ one can expect that $v_a(z) \cong v_k(z) \cong v_1(z)$ $[v_a(z) \cong v(z,(k-1)\Delta\tau) \cong v(z,0)]$. Then the mean square deviation of $v_a(z)$ from $v(z,0)$, $Dv_a(z) = \langle [v_a(z) - v(z,0)]^2\rangle = \langle \{T^{-1}\int_0^T [\tilde{v}(z,\vartheta) - \tilde{v}(z,0)]\,\mathrm{d}\vartheta\}^2\rangle$, can be estimated like above through the following sequence of relations: $Dv_a(z) = T^{-2}\sigma_v^2 \int\int_0^T \mathrm{d}\vartheta'\,\mathrm{d}\vartheta''\langle [v(z,\vartheta') - v(z,0)][v(z,\vartheta'') - v(z,0)]\rangle/\sigma_v^2 = \sigma_v^2[1 - (2/T^2)\int_0^T \theta K(\theta)\mathrm{d}\theta] \approx -\sigma_v^2 K^{II}(0)T^2/4 \sim \sigma_v^2 T^2/(4t_c^2) \ll \sigma_v^2$; here $K^{II}(0) \sim t_c^{-2}$ is the second derivative (supposed to exist) at $\theta = 0$ of the function $K(\theta)$ that is represented by the first two terms of its Taylor-series expansion, i.e. $K(\theta) = 1 + K^{II}(0)\theta^2/2$. So, in mind that $Dv_a(z) \ll \sigma_v^2$, one can now interpret $v_a(z)$, in practice, as an instantaneous Doppler-velocity profile $v_a(z) \cong v_k(z) \cong v_1(z)$. As a whole, it is seen that the above-described results from the analysis of $v_a(z)$ are in accordance with the existing conception [6, 14, 19] about the character of the Doppler-velocity profiles recovered by the inverse techniques derived on the basis of Equation (5).

## 5. Simulations

In this section we represent and discuss some results of the computer simulations we have conducted in order to reveal the features (advantages and limitations) of the algorithm performance.

The models concerned with $v_m(z)$ and $\Phi(z)$ are shown in Figures 1(*a*) and (*b*). They contain sharply-varying small-size (~50 and 75 m, respectively) inhomogeneities. The mostly employed model of the mean pulse power shape $f(\vartheta)$ is shown also in Figure 1(*b*). The effective pulse length (~150 m) is chosen to exceed the mean sizes of the inhomogeneities of $v_m(z)$ and $\Phi(z)$. The laser radiation wavelength, the temporal sampling interval, and the lidar dead-zone upper limit are chosen to be $\lambda = 2\,\mu\mathrm{m}$, $\Delta t = 0.01\,\mu\mathrm{s}$ ($\Delta z = 1.5\,\mathrm{m}$), and $z_0 = 300\,\mathrm{m}$, respectively.

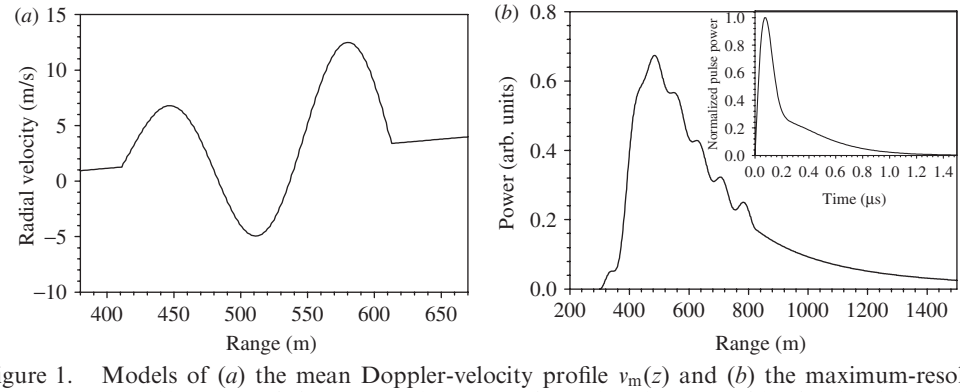


Figure 1. Models of (*a*) the mean Doppler-velocity profile $v_m(z)$ and (*b*) the maximum-resolved signal power profile $\Phi(z)$ and the mean pulse power shape $f(\vartheta)$ (inset) used in the simulations.

The realizations of the coherent lidar return signal $I(t) = J(t) + \mathrm{j}Q(t)$ are simulated according to Equation (4) taking into account the fact that because of the incoherent character of the aerosol backscattering process the polarization components of the backscattered radiation can be considered as circular complex Gaussian random quantities (see e.g. in [4,20,21]). In this case the signal $I(t = 2z/c)$ is always accompanied by a (multiplicative) speckle noise.

In order to reveal the influence on the algorithm performance of the other disturbing regular (deterministic) and random factors of importance, we have simulated additive measurement noise $n(\vartheta)$, regular frequency deviations (chirp) $\delta\omega_{\mathrm{ch}}(\vartheta)$, random pulse-shape fluctuations and spatio-temporal Doppler velocity fluctuations $\tilde{v}(z, \vartheta)$. To reveal distinctly (in a pure form) the effects of the concerned disturbing factors we consider separately each one, assuming the absence of the others. Only the speckle noise is always naturally present. Random frequency $\delta\omega_{\mathrm{r}}(\vartheta)$ and phase $\varphi_{\mathrm{r}}(\vartheta)$ fluctuations are not especially simulated here because their effect is similar to that of the Doppler-velocity fluctuations. We have not simulated fluctuations of $\Phi_{\mathrm{c}}(z)$, either. In a sense, these fluctuations should influence the retrieval process like the pulse shape fluctuations. Also, we have not especially simulated heterodyne-signal fluctuations caused by the turbulent fluctuations of the atmospheric refractive index. These fluctuations are investigated in depth and detail by simulations, e.g. in [22] and [23] where it is shown that in this case the heterodyne-power relative variance, at moderate-to-strong turbulence levels and radiation wavelengths $\lambda$ of 2 and 10.6 μm, attains a value of about 0.25. At the same time, the relative heterodyne-power variance due to speckle noise is always equal to unity. Then, the relative variance due to both effects would reach a maximum of about 1.5 corresponding to a standard deviation of 1.22. Thus, the refractive-turbulence effect may amplify to some extent the measurement error due to the speckle effect.

The covariance estimates are obtained according to the relation

$$\widehat{\mathrm{Cov}}(t, \theta = m\Delta t) = N^{-1} \sum_{k=1}^{N} [I_k(t) + n_k(t)]^* [I_k(t + m\Delta t) + n_k(t + m\Delta t)], \tag{20}$$

where $t = l\Delta t = 2l\Delta z/c$ $(l = 0, 1, 2, \ldots)$, and $N$ is the number of statistical realizations employed $I_k(t) + n_k(t)$. At $m = 0$, Equation (20) provides the estimate $\hat{P}(t) = \widehat{\mathrm{Cov}}(t, \theta = 0)$ of the signal power profile $P(t) = \mathrm{Cov}(t, \theta = 0)$. After $\hat{P}(t)$ is known, we obtain by deconvolution [8] the estimate $\hat{\Phi}(z = ct/2)$ of the short-pulse signal power profile $\Phi(z = ct/2)$.

At a sufficiently large number of laser shots the influence of most of the random factors on the retrieval accuracy will be essentially reduced. But since the number $N$ of signal realizations cannot be arbitrarily high, some type of filtering is necessary to suppress additionally the effect of the random factors. However, the filtering procedure lowers the range resolution; the characteristic resolution cell $R$ will be already of the order of the width $W$ of the window of the filter employed [6]. To retain a satisfactory range resolution, the value of $W$ should be less than the least variation scale $\Lambda_v$ of the mean radial velocity. Then the restored velocity profiles $v_{\mathrm{r}}(z)$ are minimally distorted with respect to the true ones, $v_{\mathrm{m}}(z)$. We have used in the simulations a smooth monotone sharp-cutoff digital filter [24] with a $\pi/(9\Delta t)$-wide passband for smoothing the estimates $\widehat{\mathrm{Cov}}(t, \theta)$, $\widehat{\mathrm{Cov}}(t, 0)$, and

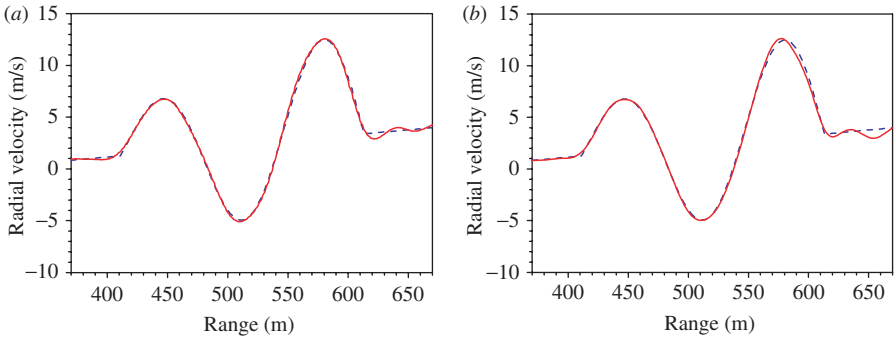


Figure 2. Doppler-velocity profiles $v_r(z)$ restored by use of (*a*) algorithm (13) and (*b*) algorithm (17) in the absence of disturbing factors except the speckle noise. The original profile $v_m(z)$ is given for comparison by the dashed curve. (The colour version of this figure is included in the online version of the journal.)

$\hat{\Phi}(z = ct/2)$, and the restored profiles $v_r(z = ct/2)$. The corresponding range resolution cell is $R \sim W = 9c\Delta t/2$ or $9\Delta z$.

Profiles of $v_r(z)$ recovered on the basis of relations (13) and (17) by using 300 and 1000 signal realizations, respectively, in the absence of additive noise and other disturbing factors but the speckle noise, are given by solid curves in Figure 2(*a*) and (*b*), respectively. As is evident, these profiles are closely coincident with the given (to be retrieved) model of $v_m(z)$ (dashed curves).

After the brief introductory information about the simulation procedures, let us further consider and discuss some concrete results from simulating the effects of different disturbing factors.

### 5.1. *Additive measurement noise*

An additive stationary random noise $n(t) = nw_n(t) = n[w_{nr}(t) + jw_{ni}(t)]$ is simulated in such a way that $\langle w_{nr}(t)\rangle = \langle w_{ni}(t)\rangle = 0$ and $\langle w^2_{nr}(t)\rangle = \langle w^2_{ni}(t)\rangle = 1/2$. Thus, $\langle n(t)\rangle = 0$, and the noise power (noise variance) $P_n = \langle |n(t)|^2\rangle = n^2$. In the case of uncorrelated noise, the covariance $\mathrm{Cov}_{w_n}[(s-q)\Delta t] = \langle w_n(t = q\Delta t)w^*_n(t = s\Delta t)\rangle$ is equal to zero for $q \neq s$. In the case of correlated noise it is chosen to have a Gaussian form, $\mathrm{Cov}_{w_n}[(s-q)\Delta t] = \exp[-(s-q)^2(\Delta t)^2/\tau^2_n]$, where $\tau_n$ is the noise correlation time. Since the in-phase and quadrature channels are statistically independent, it is implied that $\langle w_{n,r}w_{n,i}\rangle = 0$, and $\langle w_{n,r}(q\Delta t)w_{n,r}(s\Delta t)\rangle = \langle w_{n,i}(q\Delta t)w_{n,i}(s\Delta t)\rangle = (1/2)\exp[-(s-q)^2(\Delta t)^2/\tau^2_n]$. The signal-to-noise ratio (SNR) is specified as the ratio of the time-averaged signal power $P = 1/(t_2 - t_1)\int_{t_1}^{t_2} P(t)\mathrm{d}t$ to the mean noise power $P_n = n^2$; $z_1 = ct_1/2$ and $z_2 = ct_2/2$ are, respectively, the initial and the final points of the region of interest along the LOS. Certainly, the actual signal-to-noise ratio, $\mathrm{SNR_a} = P(t)/n^2$, may strongly vary with $t$ (with $z$) because of strong variations of the power $P(t)$. We suppose here that $\delta\omega_{ch}(\vartheta) \equiv 0$, $g(\vartheta) \equiv 0$, and $\tilde{v}(z) \equiv 0$.

In Figure 3(*a*) and (*b*) we have represented by solid curves the Doppler-velocity profiles $v_r(z)$ restored by use of algorithm (13) in the presence of uncorrelated additive noise at SNR = 10 and 1, respectively. (The results obtained in the presence of additive

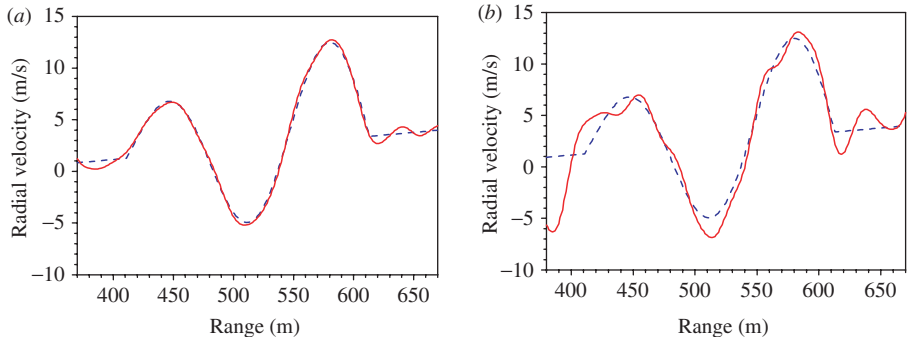


Figure 3. Doppler-velocity profiles $v_r(z)$ restored by use of algorithm (13) in the presence of uncorrelated additive noise at (*a*) SNR = 10 and (*b*) SNR = 1; $N = 300$. The original profile $v_m(z)$ is given for comparison by the dashed curve. (The colour version of this figure is included in the online version of the journal.)

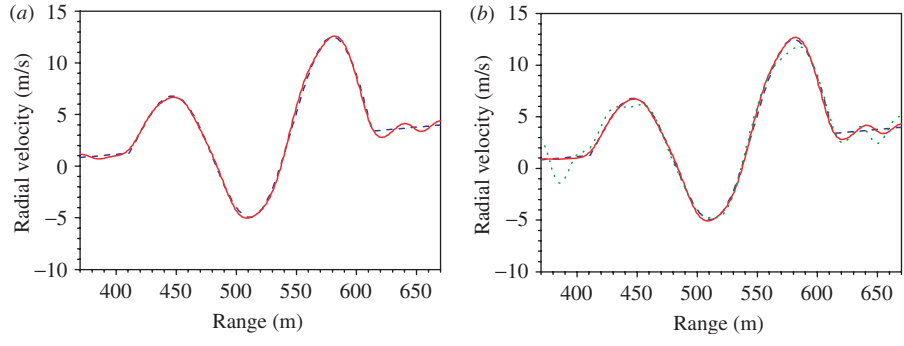


Figure 4. Doppler-velocity profiles $v_r(z)$ restored by use of algorithm (13) in the presence of correlated additive noise at (*a*) SNR = 10 ($\tau_c = 2\Delta t_0$) and (*b*) SNR = 1 [$\tau_c = 2\Delta t_0$ (dotted curve) and $\tau_c = 10\Delta t_0$ (solid curve)]; $N = 300$. The original profile $v_m(z)$ is given for comparison by the dashed curve. (The colour version of this figure is included in the online version of the journal.)

measurement noise at SNR = 100 are the same as those shown in Figure 2.) It is seen that in the former case the restored profile $v_r(z)$ is closely coincident with the model $v_m(z)$. In the latter case the profile $v_r(z)$ is distorted to a higher extent with respect to $v_m(z)$. In the presence of correlated noise the quality of the restored profiles $v_r(z)$ is better at larger noise-correlation time $\tau_c$ (see Figures 4(*a*) and (*b*)); for instance, when $\tau_c = 2\Delta t_0$ (at SNR = 10) and $\tau_c = 10\Delta t_0$ (at SNR = 1) the restored profiles $v_r(z)$ do not differ from those restored in absence of additive noise.

An additive measurement noise influences more essentially the performance of algorithm (17). For instance, to achieve the same uncorrelated-noise suppression as by algorithm (13) at SNR = 10, one should employ here $N \sim 1000$ statistical realizations. The disturbing effect of a correlated noise decreases again with the increase of $\tau_c$; when $\tau_c = 2\Delta t_0$ (at SNR = 10 and $N = 500$) and $\tau_c = 10\Delta t_0$ (at SNR = 1 and $N = 1000$) the

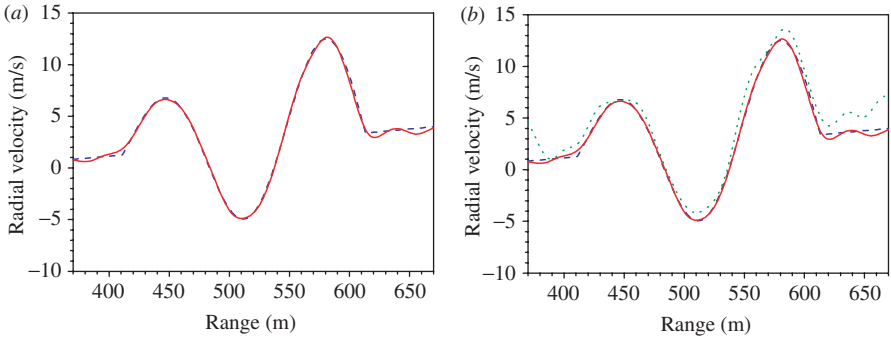


Figure 5. Doppler-velocity profiles $v_r(z)$ restored by use of algorithm (17) in the presence of correlated additive noise at (*a*) SNR = 10 ($\tau_c = 2\Delta t_0$, $N = 500$) and (*b*) SNR = 1 [$\tau_c = 2\Delta t_0$ (dotted curve) and $\tau_c = 10\Delta t_0$ (solid curve), $N = 1000$]. The original profile $v_m(z)$ is given for comparison by the dashed curve. (The colour version of this figure is included in the online version of the journal.)

profiles $v_r(z)$ do not differ essentially from those restored in the absence of additive noise (Figure 5). Decreasing the noise influence with increasing the correlation time (narrowing the bandwidth) of the noise is due to the differentiation procedure to obtain $\mathcal{R}(t)$ (see Equation (9)). Certainly, similar but more complicated (for viewable interpretation) mathematical factors condition the higher sensitivity to noise of algorithm (17).

In general, the computer simulations with uncorrelated and correlated additive measurement noise show that algorithm (13) allows one to accurately retrieve sharply varying Doppler-velocity profiles (whose variation scale is less than the pulse length) at SNR $\geq 10$, and even at SNR $\geq 1$ and $\tau_c \geq 2\Delta t_0$, when appropriate data processing is performed based on a reasonable number $N = 300$ of signal realizations. Algorithm (17) is more sensitive to uncorrelated noise, but is quite effective in the presence of correlated noise at SNR $\geq 1$, $\tau_c \geq 2\Delta t_0$, and $N = 500$–1000. The average (along the LOS) retrieval error for both the algorithms can be of the order of or less than $1\,\mathrm{ms}^{-1}$.

### 5.2. *Chirp effect*

The chirp effect on the retrieval of radial velocity profiles has been investigated in [6] for the case of exponentially-shaped sensing pulses. It is shown there that although the chirp effect is more important in $CO_2$ coherent Doppler lidars, it may also be noticeable in coherent lidars with solid-state laser transmitters whose radiation wavelength is $\lambda \sim 2\,\mu\mathrm{m}$. Here we consider just the latter case.

The frequency chirp $\delta\omega_{ch}(\vartheta) = 2\pi\delta\nu_{ch}(\vartheta)$ in the sensing laser pulse is simulated in the form represented in the insets of Figure 6, where only the minimum of the curve varies, i.e. the (negative) maximum frequency deviation $\delta\omega_{chm} = 2\pi\delta\nu_{chm}$ varies. Such a chirp form is arbitrarily chosen, in general.

For relatively small values of $\delta\omega_{chm} \sim -0.05\,\mathrm{MHz}$ the chirp influence on the retrieval accuracy is negligible. Then the Doppler-velocity profiles $v_r(z)$ restored on the basis of algorithms (13) and (17) without and with compensation for the chirp are coincident. They also coincide with the corresponding profiles $v_r(z)$ restored in the absence of

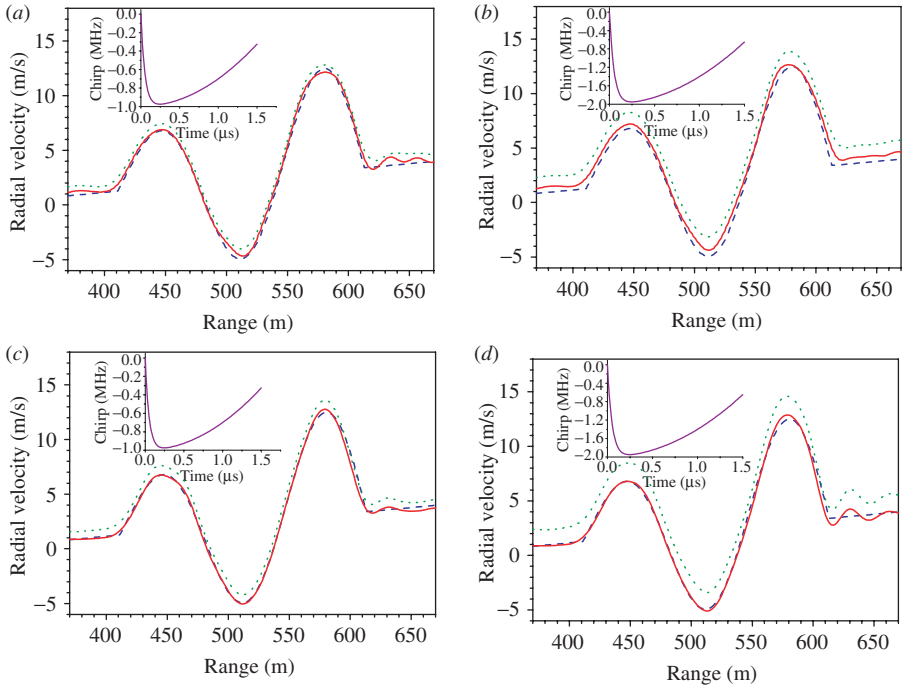


Figure 6. Doppler-velocity profiles $v_r(z)$ restored by use of algorithms (13) (*a*, *b*) and (17) (*c*, *d*) with (solid curves) and without (dotted curves) compensation for the chirp in the case of the frequency chirp given in insets, with chirp module maximum 1 MHz (*a*, *c*) and 2 MHz (*b*, *d*). The original profile $v_m(z)$ is given for comparison by the dashed curve. (The colour version of this figure is included in the online version of the journal.)

disturbing factors. For larger values of $\delta\omega_{chm} \sim -1$ MHz and $-2$ MHz, the neglect of the correction for the chirp in the retrieval algorithms leads to the appearance of a (certainly positive, shift up) bias error in the determination of $v_r(z)$. This error is compensated for when the chirp effect is taken into account in the retrieval algorithms (see Figure 6).

### 5.3. *Pulse shape fluctuations*

Although algorithms (13) and (17) are, in general, in power for non-stationary pulse shape fluctuations, we have simulated here stationary ones. This allows one to avoid unnecessary complications without any loss of generality. Assuming that $n(\vartheta) \equiv 0$, $\delta\omega_{ch}(\vartheta) \equiv 0$, and $\tilde{v}(z) \equiv 0$, the pulse-power shape fluctuations are simulated through the relative pulse envelope fluctuations $\kappa(\vartheta)$ (see Equation (2)). Correspondingly, the mean pulse power shape is given by Equation (3b). The relative standard deviation of the pulse power is then $\sim 2[\eta(\vartheta)]^{1/2} = 2\langle\kappa^2(\vartheta)\rangle^{1/2}$. When the power shape is estimated on the basis of a large number $N \gg 1$ of statistical realizations, the standard deviation is reduced to $\sim 2[\eta(\vartheta)/N]^{1/2}$. For stationary fluctuations the value of $\eta$ is constant and determines a fluctuation level independent of $\vartheta$. The random function $\kappa(\vartheta)$ is simulated either as uncorrelated noise or as a correlated one having a correlation time exceeding or less than

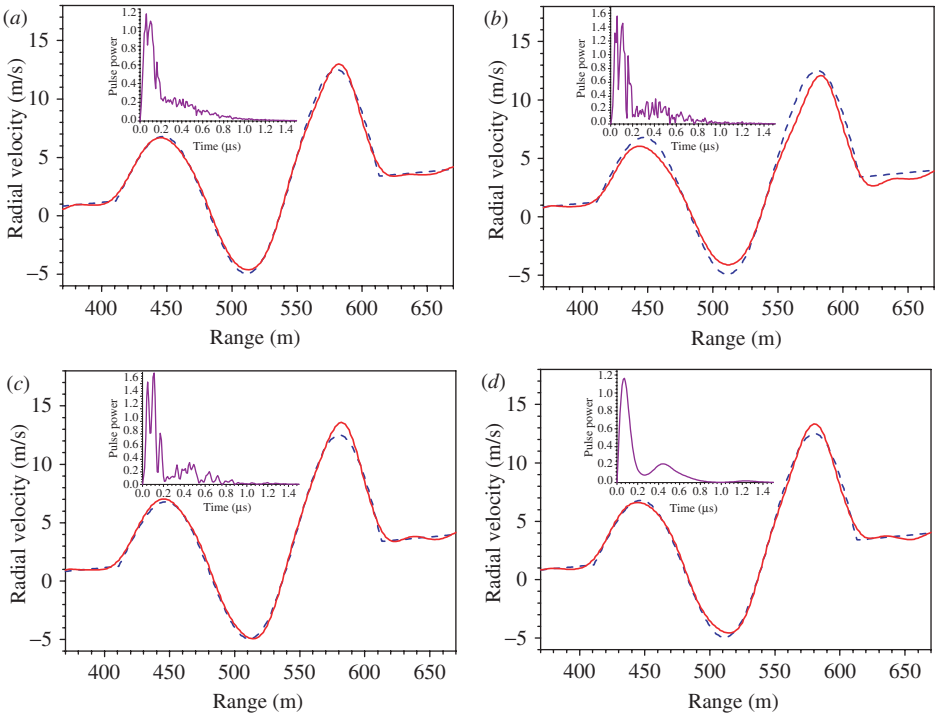


Figure 7. Doppler-velocity profiles $v_r(z)$ restored by use of algorithm (13) in the presence of pulse shape fluctuations with (*a*) $\kappa = 0.1$, (*b*) $\kappa = 0.3$, (*c*) $\kappa = 0.3$, $\tau_c = 2\Delta t_0$ and (*d*) $\kappa = 0.3$, $\tau_c = 20\Delta t_0$. Inset – one realization of the pulse shape. The mean pulse shape employed is obtained by averaging over 300 pulse realizations. The original profile $v_m(z)$ is given for comparison by the dashed curve. (The colour version of this figure is included in the online version of the journal.)

the pulse duration. The simulations show that a mean pulse shape obtained by averaging over a sufficiently large number of realizations $N$ (e.g. $N = 300$ or $N = 500$) ensures accurate determination of $v_r(z)$ by algorithms (13) and (17), independently of the statistics of $\kappa(\vartheta)$. Certainly, the less the value of $\eta$ the higher the retrieval accuracy. Some results from applying algorithm (13) are illustrated in Figure 7. Similar results are obtained as well on the basis of algorithm (17).

### 5.4. *Turbulent velocity fluctuations*

The radial velocity fluctuations $\tilde{v}(z, \vartheta)$ are simulated as normally distributed zero-mean spatio-temporal turbulent fluctuations, whose autocovariance is

$$\mathrm{Cov}_v(\rho_z, \tau) = \langle \tilde{v}(z, \vartheta)\tilde{v}(z + \rho_z, \vartheta + \tau)\rangle = \mathrm{Cov}_v(|\rho_z - V\tau|)\exp(-\tau^2/\tau_l^2), \tag{21a}$$

where

$$\mathrm{Cov}_v(\rho) = 0.25C^2\varepsilon^{2/3}\int_0^\infty \mathrm{d}K\,\cos(K\rho)(K^2 + K_o^2)^{-5/6}\exp(-K^2/K_m^2), \tag{21b}$$

$C^2 = 1.77$, $\varepsilon$ is the turbulent-energy loss rate, $K_o = 1/L_o$, $L_o$ is the outer turbulence scale, $K_m = 5.92/l_m$, $l_m = l_o(15C^2)^{3/4}$, $l_o$ is the inner turbulence scale; the quantities $V$ and $\tau_l$ are considered, respectively, as a mean longitudinal (along the LOS) drift velocity and an effective lifetime of the turbulence inhomogeneities (whirls). The structure function, $D_{zz}(\rho) = 2[\mathrm{Cov}_v(0) - \mathrm{Cov}_v(\rho)]$ corresponding to $\mathrm{Cov}_v(\rho)$ is a compact and accurate approximation (over the corresponding ranges of definition) of the well-known Kolmogorov–Obukhov radial structure function [13]. When $\rho \gg L_o$, function $D_{zz} = 2\sigma_v^2 = C^2(\varepsilon L_o)^{2/3}$, i.e. the radial-velocity standard deviation $\sigma_v = \mathrm{Cov}(0) = \langle \tilde{v}^2 \rangle^{1/2} = C(\varepsilon L_o)^{1/3}/2^{1/2} \approx (\varepsilon L_o)^{1/3}$. A similar expression for $\sigma_v$ is obtainable on the basis of a more rigorous theoretical estimation [13]. The model chosen of the autocovariance $\mathrm{Cov}_v(\rho_z, \tau)$ (Equation (21a)) is somewhat simplified. It describes, in practice, an entirely radial drift of the turbulent whirls and contains only one temporal scale $\tau_l$. At the same time such a model is quite realistic because the radial drift is a quite possible experimental case, and $\tau_l$ can be interpreted as the (superior) lifetime of the largest turbulence scales that determine the largest velocity fluctuations. Thus, the autocovariance model contains the main features of a turbulent velocity fluctuation field concerning the correlation transfer and decay.

The discretized realizations of the radial-velocity fluctuation field are modelled in the way described in Appendix 1. The basic modelling parameters used in the simulations are: $\sigma_v = 4\,\mathrm{ms}^{-1}$; $V = 5\,\mathrm{ms}^{-1}$; $L_0 = 20\,\mathrm{m}$ and $l_0 = 0.001\,\mathrm{m}$; $\tau_l = 5\,\mathrm{s}$; $\Delta z = 1.5\,\mathrm{m}$; and (see below) $\Delta t_\perp = 0.01\,\mathrm{s}$. Then the velocity fluctuation correlation time is $t_c \sim \min[\tau_l, L_0/V] \sim 4 - 5\,\mathrm{s}$. The realizations $\omega_{\mathrm{im},k}(z_l) = \omega_0[1 - 2v_k(z_l)/c] - \omega_h$ of the profile $\omega_{\mathrm{im}}(z)$ of the intermediate frequency at each ($k$th) laser shot (see Equation (4)) are generated through the corresponding realizations $v_k(z_l)$ of the Doppler-velocity profile $v(z)$. Each realization of $v_k(z_l)$ is considered as a sum $v_k(z_l) = v_m(z_l) + \tilde{v}_k(z_l)$ of the ensemble-mean Doppler-velocity profile $v_m(z_l) = \langle v(z_l) \rangle$ and the profile of the turbulent velocity fluctuations $\tilde{v}_k(z_l)$. The realizations $\tilde{v}_k(z_l)$ are extracted from the statistically-generated velocity fluctuation field $\tilde{v}(l, m) = \tilde{v}(z_l = l\Delta z, t_\perp = m\Delta t_\perp)$ $(l, m = 0, 1, 2, \ldots)$, where $t_\perp$ is the current measurement time, and $\Delta t_\perp$ is the corresponding sampling interval. In this case we have $\tilde{v}_k(z_l) \equiv v[(l-1)\Delta z, (k-1)q\Delta t_\perp]$ $(l, k = 1, 2, \ldots)$, where $q$ is an integer, and $q\Delta t_\perp$ is the interval between the adjacent laser shots. The short-term ($T \ll t_c$), mid-term $T \sim t_c$, and long-term $T \gg t_c$ lidar measurement procedures are simulated by appropriate choice of the interval $q\Delta t_\perp$. So we have simulated, respectively, $N = 300$, 200, and 140 laser shots produced within measurement intervals $T = 1.2$, 4, and 280 s. The corresponding restored Doppler-velocity profiles $v_r(z)$ are shown together and compared in Figure 8(*a*)–(*c*) with the arithmetic-mean profile $v_a(z)$, the ensemble-mean profile $v_m(z)$, and the profile $v_1(z) = v_m(z) + \tilde{v}_1(z)$ at only one (say, the first, $k = 1$) laser shot. It is seen that the results from the simulations confirm the pre-visions about the character of the recovered profiles. So, in all the cases the profile $v_r(z)$ closely fits $v_a(z)$ (see Equation (18)). In the case of a short-term measurement (Figure 8(*a*)) the profile $v_r(z)$, being in general different from $v_m(z)$, is near each profile $v_k(z)$. At a mid-term measurement procedure (Figure 8(*b*)) the profile $v_r(z)$ may differ from both $v_m(z)$ and $v_k(z)$. At a long-term measurement (Figure 8(*c*)) the restored profile $v_r(z)$ may differ in general from $v_k(z)$, but nearly approximates $v_m(z)$. In the last case, according to the law of averages, $v_a(z)[\sim v_r(z)]$ should tend to $v_m(z)$ when $N > T/t_c \gg 1$.

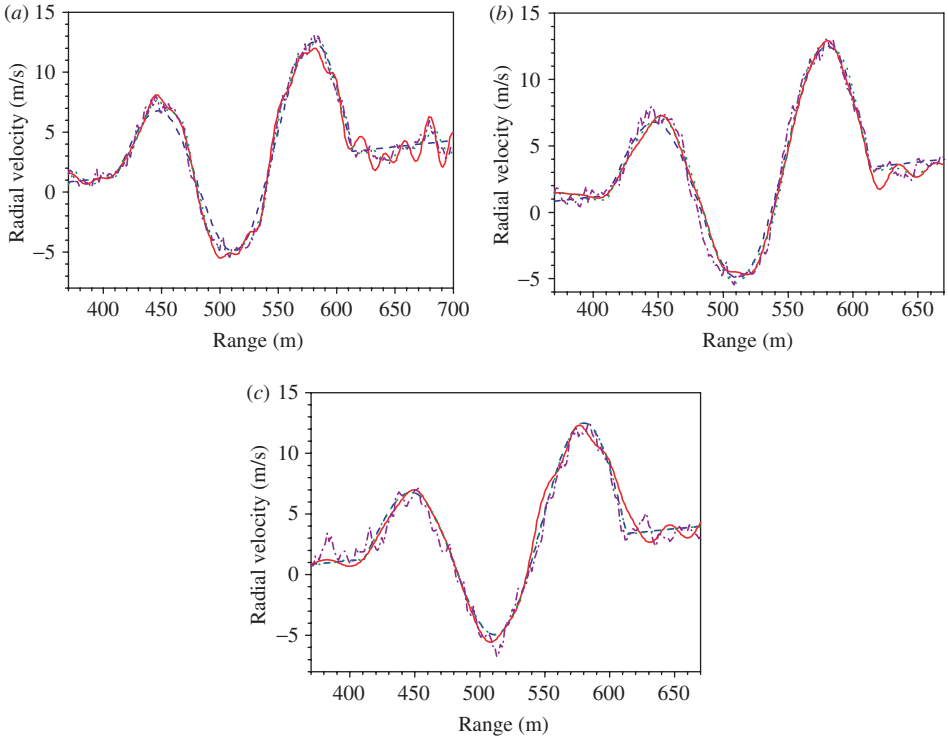


Figure 8. Comparison of restored Doppler-velocity profiles $v_r(z)$ (solid curves) with the ensemble-mean profiles $v_m(z)$ (dashed curves), the arithmetic-mean profiles $v_a(z)$ (dotted curves) and the instantaneous profile $v_1(z)$ (dashed-dotted curve) in the cases of short-term (*a*), middle-term (*b*) and long-term (*c*) measurement procedures. (The colour version of this figure is included in the online version of the journal.)

## 6. Conclusion

In the present work we have developed general-enough inverse mathematical techniques for high-resolution retrieval of Doppler-velocity profiles on the basis of coherent heterodyne pulsed lidar data. These techniques are based on the analysis of the complex heterodyne signal autocovariance represented in a general form, taking into account the random phase and frequency fluctuations and the regular frequency deviation in the sensing laser pulses, the pulse-shape fluctuations, and the fluctuations of the radial velocity of the aerosol scatterers. The algorithms obtained are valid at arbitrary frequency chirp, arbitrary pulse shapes and non-stationary pulse-shape fluctuations. They allow one in principle to determine the Doppler-velocity profiles with a resolution cell of the order of the sampling interval. However, the real achievable resolution cell is larger because of the necessity of digital filtering procedures for additionally suppressing the influence of various random factors such as additive measurement noise, pulse shape fluctuations, and frequency or phase fluctuations caused e.g. by turbulent velocity fluctuations. The effects of these factors have been investigated by computer simulations. So, except for

the speckle noise that is always present, uncorrelated and correlated additive noise has also been simulated. It is shown in this case that, by using appropriate filtering procedures, one can satisfactorily restore sharply varying velocity profiles at a reasonable number of signal realizations, e.g. $N = 300$ for Fourier retrieval or $N = 1000$ for Volterra retrieval. The achievable accuracy may be of the order of 1–2 $ms^{-1}$ at a SNR of the order of unity. Stationary pulse shape fluctuations have been simulated as well as having small or large correlation time as compared with the pulse duration. The simulations show that a mean pulse shape, used in the retrieval algorithms, averaged over a sufficiently large number of pulse realizations $N$ (e.g. $N = 300$ or $N = 1000$) allows one to recover accurately the Doppler-velocity profiles, independently of the fluctuation correlation time. Certainly, the lower the fluctuation level, the higher the retrieval accuracy and the less the required number of pulse realizations. The simulations performed of arbitrary in form regular frequency deviations in the sensing laser pulse illustrate the compensation for the chirp-due bias error when the chirp correction terms in algorithms (13) and (17) are taken into account. The simulations of turbulent spatio-temporal radial-velocity fluctuations confirm the analytical theoretical predictions that at long-term measurements, under stationary atmospheric conditions, when $T \gg t_c$, the recovered velocity profile is an estimate of the ensemble-mean Doppler-velocity profile $v_m(z)$. For a short-term measurement procedure, when $T \ll t_c$, it should coincide with a near instantaneous Doppler-velocity profile, i.e. $v_a(z) \cong v_1(z) \cong v_k(z)$. In general, when $T \sim t_c$, we obtain a mean, for the period $T$, range-resolved Doppler-velocity profile $v_a(z)$.

As a whole, the simulations performed show that the inverse techniques developed in this work allow one to retrieve accurately Doppler-velocity profiles with a resolution cell that is essentially smaller than the pulse length. The retrieval error due to the combined action of the above-described disturbing factors can be reduced by appropriate bias-compensating approaches, filtering procedures and statistical averaging, to the order of 1–2$ms^{-1}$. Finally, it is important to note again that even under variable atmospheric conditions, the retrieval algorithms developed here lead to a clearly interpretable result that is the mean for the observation time, but range-resolved Doppler-velocity profile.

## Acknowledgements

This research was partially supported by the Bulgarian National Science Fund under project No. F-1511.

## References

[1] Post, M.J.; Cupp, R.E. *Appl. Opt.* **1990,** *29,* 4145–4158.
[2] Lottman, B.T.; Frehlich, R. *Appl. Opt.* **1998,** *37,* 8297–8305.
[3] Hannon, S.M.; Thomson, J.A. *J. Mod. Opt.* **1994,** *41,* 2175–2196.
[4] Gurdev, L.L.; Dreischuh, T.N.; Stoyanov, D.V. *J. Opt. Soc Am. A* **2001,** *18,* 134–142.
[5] Gurdev, L.L.; Dreischuh, T.N.; Stoyanov, D.V. *Appl. Opt.* **2002,** *41,* 1741–1749.
[6] Gurdev, L.L.; Dreischuh, T.N. *Opt. Commun.* **2003,** *219,* 101–116.
[7] Goodman, J.W.; *Statistical Optics*; Wiley: New York, 1985.
[8] Gurdev, L.L.; Dreischuh, T.N.; Stoyanov, D.V. *J. Opt. Soc. Am. A* **1993,** *10,* 2296–2306.
[9] Gurdev, L.L.; Dreischuh, T.N.; Stoyanov, D.V. *Opt. Commun.* **1998,** *151,* 339–352.

[10] Hardesty, R.M.; Keeler, R.J.; Post, M.J.; Richter, R.A. *Appl. Opt.* **1981,** *20,* 3763–3769.
[11] Belmonte, A.; Rye, B.J. *Appl. Opt.* **2000,** *29,* 2401–2411.
[12] Samokhvalov, I.V., Ed. *Correlation Methods of Laser-Location Mesurements of Wind Velocity*; Nauka, Novosibirsk, 1985.
[13] Tatarski, V.I. *Wave Propagation in Turbulent Atmosphere*; Nauka: Moscow, 1967.
[14] Gurdev, L.L.; Dreischuh, T.N. *Proc. SPIE* **2003,** *5226,* 300–304.
[15] Gurdev, L.L.; Dreischuh, T.N. *Proc. SPIE* **2003,** *5226,* 310–314.
[16] Pearson, G.N. *Rev. Sci. Instrum.* **1993,** *64,* 1155–1157.
[17] Volterra, V. *Theory of Functionals and of Integral and of Integro-Differential Equations*; Dover: New York, 1958.
[18] Hudson, D.J. *Lectures on Elementary Statistics and Probability*; CERN: Geneva, 1963.
[19] Gurdev, L.L.; Dreischuh, T.N. *Proc. SPIE* **2005,** *5830,* 332–336.
[20] Salamitou, Ph.; Dabas, A.; Flamant, P. *Appl. Opt.* **1995,** *34,* 499–506.
[21] Bronstein, I.N.; Semendjajew, K.A. *Taschenbuch der Mathematik*; Nauka: Moscau; BSB B.G. Teubner: Leipzig, 1989.
[22] Belmonte, A. *Opt. Express* **2004,** *12,* 168–175.
[23] Belmonte, A. *Opt. Express* **2005,** *13,* 9598–9604.
[24] Hamming, R.W. *Digital Filters*; Prentice-Hall: Englewood Cliffs, NJ, 1983.

## Appendix

### A1. Modelling spatio-temporal turbulent radial-velocity fluctuations

The task to be solved here is to model a statistically stationary and homogeneous spatio-temporal random field of normally distributed zero-mean radial-velocity fluctuations with some determinate (turbulence-conditioned) correlation properties. The only spatial coordinate concerned in this case is the range $z$ along the lidar LOS. The temporal coordinate (marking in particular the instants of emitting the sensing laser pulses) will be denoted by $t_\perp$ in order to be distinguished from the time $t$ after the pulse emission. Let us also note that the computer modelling presumes spatial and temporal sampling with intervals (sampling steps) $\Delta z$ and $\Delta t_\perp$, respectively. A way chosen here of solving the above-formulated task is to perform appropriate two-dimensional digital filtration of a suitable uncorrelated spatio-temporal random field. The digital filter employed should be designed in such a way that the resultant random field (after the filtration) has the necessary spectrum corresponding to the desired spatio-temporal autocovariance.

It is expedient to generate, as an initial random field (to be filtered), a spatio-temporal normally-distributed discrete white noise with unitary variance, $W_\mathrm{d}(z = l\Delta z, t_\perp = m\Delta t_\perp) \equiv W_\mathrm{d}(l, m)$ $(l, m = 0, 1, 2, \ldots)$, representing the discrete samples of a spectrally-limited continuous white noise $W_\mathrm{c}(z, t_\perp)$ with boundary wavenumber $K_\mathrm{b} = \pi/\Delta z$ and boundary frequency $\omega_\mathrm{b} = \pi/\Delta t_\perp$. To convert $W_\mathrm{c}(z, t_\perp)$ into a velocity fluctuation field $\tilde{v}(z, t_\perp)$ with some required spectrum (autocovariance) one can use appropriate linear transformation (filtration),

$$\begin{aligned}\tilde{v}(z, t_\perp) &= \int\int_{-\infty}^{\infty} \mathrm{d}z'\mathrm{d}t'_\perp\, h(z - z', t_\perp - t'_\perp) W_\mathrm{c}(z', t'_\perp) \\ &= \int\int_{-\infty}^{\infty} \mathrm{d}z'\mathrm{d}t'_\perp\, h(z', t'_\perp) W_\mathrm{c}(z - z', t_\perp - t'_\perp),\end{aligned} \tag{22}$$

with a transition function $h(z', t'_\perp)$ whose discrete values $h(n, i) \equiv h(n\Delta z, i\Delta t_\perp)$ are connected with the elements (the coefficients to be determined below) $C_{ni}$ of the filtering matrix $C = \{C_{ni}\}$. The discrete values $\tilde{v}(l, m) \equiv \tilde{v}(l\Delta z, m\Delta t_\perp)$ of the desirable velocity fluctuation field are expressible as

$$\tilde{v}(l, m) = \sum_{n,\, i=-\infty}^{\infty} C_{ni} W_\mathrm{d}(l - n, m - i). \tag{23}$$

To avoid noticeable distortions due to discretization, we suppose that the boundary wavenumber and frequency, $K_b$ and $\omega_b$, exceed the corresponding upper wavenumber and frequency limits of the power spectrum $\Phi_v(K,\omega)$ of $\tilde{v}(z,t_\perp)$ and the spectrum $H(K,\omega)$ of $h(z,t_\perp)$. That is, the sampling intervals $\Delta z$ and $\Delta t_\perp$ are supposed to be much less, respectively, than the characteristic spatial and temporal scales of $h(z,t_\perp)$ and the correlation radius $\rho_c$ and time $\tau_c$ of $\tilde{v}(z,t_\perp)$. The power spectrum $\Phi_v(K,\omega)$ is given by the expression

$$\Phi_v(K,\omega) = \int\int_{-\infty}^{\infty} \mathrm{d}\rho\,\mathrm{d}\tau\,\mathrm{Cov}_v(\rho,\tau)\exp[\mathrm{j}(\omega\tau - K\rho)], \tag{24}$$

where (under the condition of isotropic, locally homogeneous and stationary turbulence) the velocity fluctuation autocovariance is $\mathrm{Cov}_v(\rho,\tau) = \langle\tilde{v}(z'',t''_\perp)\tilde{v}(z',t'_\perp)\rangle$, and $\rho = z' - z''$ and $\tau = t'_\perp - t''_\perp$. The white-noise power spectrum $\Phi_w(K,\omega) = \Phi_w$ (i.e. it is uniform) for $K \in [-K_b, K_b]$ and $\omega \in [-\omega_b, \omega_b]$, and $\Phi_w(K,\omega) \equiv 0$ elsewhere. Taking into account that the noise variance $\sigma_w^2 = 1 = (2\pi)^{-2}\int\int_{-\infty}^{\infty}\mathrm{d}K\,\mathrm{d}\omega\Phi_w(K,\omega) = (2\pi)^{-2}\int_{-K_b}^{K_b}\mathrm{d}K\int_{-\omega_b}^{\omega_b}\mathrm{d}\omega\Phi_w = \Phi_w/(\Delta z\Delta t_\perp)$, we obtain that

$$\Phi_w = \Delta z\Delta t_\perp. \tag{25}$$

The spectrum $H(K,\omega)$ of the transition function $h(z,t_\perp)$ is given as

$$H(K,\omega) = \int\int_{-\infty}^{\infty}\mathrm{d}z\,\mathrm{d}t_\perp\,h(z,t_\perp)\exp[\mathrm{j}(\omega t_\perp - Kz)]. \tag{26}$$

On the basis of Equation (22) we obtain that

$$\begin{aligned}\mathrm{Cov}_v(\rho,\tau) &= \langle\tilde{v}(z+\rho,t_\perp+\tau)\tilde{v}(z,t_\perp)\rangle \\ &= \int\int\int\int_{-\infty}^{\infty}\mathrm{d}z'\,\mathrm{d}z''\,\mathrm{d}t'_\perp\,\mathrm{d}t''_\perp h(z+\rho-z',t_\perp+\tau-t'_\perp) \\ &\quad\times h(z-z'',t_\perp-t''_\perp)\,\mathrm{Cov}_w(z'-z'',t'_\perp-t''_\perp),\end{aligned} \tag{27}$$

where $\mathrm{Cov}_w(z'-z'',t'_\perp-t''_\perp) = \langle W_c(z',t'_\perp)W_c(z'',t''_\perp)\rangle$ is the white-noise autocovariance. After the change of variables $z+\rho-z' = u'$, $z-z'' = u''$, $t_\perp+\tau-t'_\perp = v'$, and $\tau - t''_\perp = v''$, Equation (27) acquires the form

$$\begin{aligned}\mathrm{Cov}_v(\rho,\tau) &= \int\int\int\int_{-\infty}^{\infty}\mathrm{d}u'\,\mathrm{d}u''\,\mathrm{d}v'\,\mathrm{d}v''h(u',v')h(u'',v'') \\ &\quad\times\mathrm{Cov}_w[\rho-(u'-u''),\tau-(v'-v'')].\end{aligned} \tag{28}$$

The Fourier transformation of Equation (28), with respect to $\rho$ and $\tau$, leads to the relation

$$\Phi_v(K,\omega) = |H(K,\omega)|^2\Phi_w = |H(K,\omega)|^2\Delta z\Delta t_\perp, \tag{29}$$

where, in general, $\Phi_w(K,\omega) = \int\int_{-\infty}^{\infty}\mathrm{d}\rho\,\mathrm{d}\tau\,\mathrm{Cov}_w(\rho,\tau)\exp[\mathrm{j}(\omega\tau - K\rho)]$. Equation (29) shows that there may be many transfer functions $H(K,\omega)$, differing only in phase, that ensure the desirable spectrum $\Phi_v(K,\omega)$. It is expedient to use the simplest of them,

$$H(K,\omega) = [\Phi_v(K,\omega)/\Phi_w]^{1/2}, \tag{30}$$

having zero phase. Then the transition function $h(z,t_\perp)$ will have the form

$$h(z,t_\perp) = (2\pi)^{-2}\int_{-\omega_b}^{\omega_b}\mathrm{d}\omega\int_{-K_b}^{K_b}\mathrm{d}K[\Phi_v(K,\omega)/\Phi_w]^{1/2}\exp[\mathrm{j}(\omega t_\perp - Kz]. \tag{31}$$

Let us further represent $W_c(z-z', t_\perp - t'_\perp)$ through the following double Shannon series:

$$W_c(z-z', t_\perp - t'_\perp) = (4K_b\omega_b)^{-1} \sum_{n,\,i=-\infty}^{\infty} W_d(n,i) \int_{-K_b}^{K_b} dK \int_{-\omega_b}^{\omega_b} d\omega \times \exp\{j[\omega(t_\perp - t'_\perp - i\Delta t_\perp) - K(z-z'-n\Delta z)]\}. \quad (32)$$

Then, taking into account in Equation (22) the expressions of Equations (31) and (32), we obtain that

$$\tilde{v}(l,m) = \sum_{n',\,i'=-\infty}^{\infty} C_{l-n',\,m-i'} W_d(n', i'), \quad (33)$$

where

$$C_{l-n',\,m-i'} = (4K_b\omega_b)^{-1} \int_{-K_b}^{K_b} dK \int_{-\omega_b}^{\omega_b} d\omega\, [\Phi_v(K,\omega)/\Phi_w]^{1/2} \times \exp\{j[\omega(m-i')\Delta t_\perp - K(l-n')\Delta z]\}. \quad (34)$$

The change of indices, $l-n'=n$ and $m-i'=i$, in Equations (33) and (34) leads to the relations:

$$\tilde{v}(l,m) = \sum_{n,\,i=-\infty}^{\infty} C_{n,i} W_d(l-n, m-i), \quad (35)$$

where

$$C_{n,i} = (4K_b\omega_b)^{-1} \int_{-K_b}^{K_b} dK \int_{-\omega_b}^{\omega_b} d\omega\, [\Phi_v(K,\omega)/\Phi_w]^{1/2} \exp\{j[\omega\, i\, \Delta t_\perp - Kn\Delta z]\}. \quad (36)$$

From Equation (35) it follows that $\sum_{n,\,i=-\infty}^{\infty} C_{n,i}^2 = \sigma_v^2 = \langle \tilde{v}^2 \rangle$. The same result is obtainable on the basis of Equation (36) taking into account that $\sum_{n,\,i=-\infty}^{\infty} \exp\{j[i(\omega-\omega')\Delta t_\perp - n(K-K')\Delta z]\} = \lim_{N\to\infty} \{\sin[(N-1/2)\Delta t_\perp(\omega-\omega')]\ \sin[(N-1/2)\Delta z(K-K')]/\sin[\Delta t_\perp(\omega-\omega')/2]\ \sin[\Delta z(K-K')/2]\} = [(2\pi)^2/(\Delta z \Delta t_\perp)]\ \ \delta(K-K')\delta(\omega-\omega')$, and $\int_{-K_b}^{K_b} dK \int_{-\omega_b}^{\omega_b} d\ \omega \Phi_v(K,\omega) = \sigma_v^2$. By using the above representation of $\delta(K-K')\delta(\omega-\omega')$, it is not difficult to deduce on the basis of Equation (32) that the spectrum $\Phi_w(K,\omega)$ of the noise $W_c(z, t_\perp)$ is really restricted within the rectangle $\{-K_b \le K \le K_b,\ -\omega_b \le \omega \le \omega_b\}$ being uniform and equal to $\Delta z \Delta t_\perp$.

Let us now determine explicitly the filtering matrix elements (coefficients) $C_{n,i}$ leading to the spatio-temporal velocity fluctuation autocovariance given by Equation (21a) in the principal text. The fluctuation spectrum in this case is obtained through Equation (24) in the form

$$\Phi_v(K,\omega) = \pi^{1/2}\tau_l f(K) \exp[-(\omega - KV)^2\tau_l^2/4], \quad (37)$$

where

$$f(K) = \int_{-\infty}^{\infty} d\rho\, \mathrm{Cov}_v(\rho) \exp(jK\rho) \quad (38)$$

is the spatial spectrum corresponding to the spatial autocovariance $\mathrm{Cov}_v(\rho)$ given by Equation (21b). The explicit form of $f(K)$ is

$$f(K) = 0.25\pi C^2 \varepsilon^{2/3} (K^2 + K_0^2)^{-5/6} \exp(-K^2/K_m^2). \quad (39)$$

On the basis of Equation (36), taking into account Equations (37), (39), and (25), we obtain the following (normalized to $\sigma_v$) expressions of the filtering coefficients:

$$c_{n,i} = C_{n,i}/\sigma_v = \pi^{-7/4}(\xi \Delta z \Delta t_\perp \tau_l/16)^{1/2} \int_{-\pi/\Delta z}^{\pi/\Delta z} \mathrm{d}K \int_{-\pi/\Delta t_\perp}^{\pi/\Delta t_\perp} \mathrm{d}\omega \times \exp[\mathrm{j}(\omega i \Delta t_\perp - Kn\Delta z)](K^2 + K_\mathrm{o}^2)^{-5/12} \times \exp[-K^2/(2K_m^2) - (\omega - KV)^2 \tau_l^2/8], \quad (40)$$

where $\xi = \pi / \int_0^\infty \mathrm{d}K(K^2 + K_\mathrm{o}^2)^{-5/6} \exp(-K^2/K_m^2)$. On the basis of Equation (40) one can show again analytically that $\sum_{n,i=-\infty}^{\infty} c_{n,i}^2 = 1$, i.e. $\sum_{n,i=-\infty}^{\infty} C_{n,i}^2 = \sigma_v^2$. The numerical tests also confirm this property of $c_{n,i}$ ($C_{n,i}$). Thus, the desirable discretized spatio-temporal realizations of turbulent velocity fluctuation field $\tilde{v}(l, m)$ can be generated according to algorithm (23) by using the filtering matrix $\{C_{n,i}\} = \sigma_v\{c_{n,i}\}$.